# Liquid dispersion in packed columns: Experiments and numerical modeling

M. Fourati [a,b], V. Roig [a], L. Raynal [b,*]

[a] IMFT, Université de Toulouse (INPT, UPS) & CNRS, Allée Camille Soula, 31400 Toulouse, France
[b] IFP Energies nouvelles, Rond-point de l'échangeur de Solaize BP3, 69360 Solaize, France

## HIGHLIGHTS

- Original measurements of liquid dispersion in a counter-current packed bed equipped with a modern high efficiency packing.
- Using a high resolution gamma ray system in a column of large size diameter.
- The development of closure laws that further enable CFD modeling which takes dispersion into account.
- Comparison between experiments and CFD calculations.

*Keywords:*
$CO_2$ capture
Distillation
Packing
Two-phase flow
Liquid dispersion
CFD

## ABSTRACT

In order to optimize the design of gas–liquid packed columns used in distillation or in absorption processes, it is of high importance to be able to predict liquid dispersion. Indeed, dispersion phenomena will impact the choice and design of liquid distributing devices and the height of the packed beds. For this, one mainly relies on industrial feedback and on some experimental results obtained at laboratory scale which cannot be directly extrapolated since their geometric characteristics are at least one order of magnitude less than industrial columns in terms of columns diameter and height. To fill this gap CFD simulation tools should be more used since they can apply to any scale. However the latter option requires adequate modeling in particular for dispersion forces which are little studied due to the lack of data for validation. The present paper aims at developing, from original dispersion experimental measurements, closure laws that can be implemented in CFD codes. Liquid spreading from a source point has been investigated for Mellapak 250.X packing via gamma-ray tomography measurements. Closure laws are discussed from a simple 1D model which enables to go further within the Eulerian two-fluid framework with original user-defined functions and associated models that take into account liquid dispersion in the packed bed. The latter is modeled as a porous medium with appropriate closure laws. The comparison between experiments and CFD results shows that the present approach is adequate and should be further developed in order to be more precise and adapted to more packings.

## 1. Introduction

$CO_2$ capture and storage (CCS) is known to be a possible technology for carbon mitigation. IEA (2009) considers that it could handle up to 19% of $CO_2$ emissions. Post-combustion capture using chemical solvents is one promising solution, especially when applied to coal-fired power plants, the largest industrial $CO_2$ emitters. However, the deployment of this technology requires process optimization with associated cost reduction, both in terms of operational expenditures (Opex) and capital expenditures (Capex). As underlined by Raynal et al. (2011), many studies are dedicated to new solvents identification, with the primary goal of reducing Opex, but less work deals with Capex reduction. The latter objective can be achieved by developing new high performance packings (Alix and Raynal, 2008; Alix et al., 2011; Menon and Duss, 2011) and/or by achieving the most adequate design of packed columns. Such an optimum design is linked to the choice of packing, the number of packed beds and their height, the interaction between gas and liquid distributors with the gas/liquid flow within the packed bed. All these technical choices are strongly linked to liquid dispersion and gas/liquid interaction in the packed bed but it is today mostly given by industrial experience and little comes from more scientific explanations and deterministic calculations. To take all these phenomena into account for application to very large scale absorbers ($CO_2$ absorber are expected to be in the range of 8–14 m in diameter

* Corresponding author. Tel.: +33 4 37 70 25 27; fax: +33 4 37 70 20 09.
*E-mail address:* ludovic.raynal@ifpen.fr (L. Raynal).

one order of magnitude above what can be done at laboratory scale), large scale two-fluid CFD simulations seem an appropriate tool. Some studies have started to focus on such aspects (Raynal and Royon-Lebeaud, 2007; Lappalainen et al., 2009a), but they either do not take into account liquid dispersion or are restricted to catalytic beds which geometry significantly differs from modern packings. Present article deals with liquid dispersion in modern high efficiency metallic packings.

Recent experiments performed to characterize the dispersion of liquid in a counter-current gas–liquid packed column filled with structured packings are briefly reported and discussed in part 2. We then present the hydrodynamic model used to simulate the flow in the column (part 3). It is an Eulerian two-fluid model in which we include a specific model for liquid dispersion. The global model is discussed to analyze the physics associated to the various closure laws. We also discuss the consistency of the model as well as the connection between experiments and modeling. In part 4 experimental results and numerical simulations are compared.

## 2. Experiments

In order to study the liquid dispersion, liquid distribution measurements have been performed with a high resolution tomographic system in a 400 mm diameter column of 1.5 m in height. The gas/liquid packed column is filled with Mellapak 250.X structured packing (geometric area per unit volume $a_g=250\ m^2/m^3$, porosity $\varepsilon=0.98$ and angle of the flow channels with horizontal direction $\theta=60^\circ$). It is operated in the counter-current flow mode. Liquid is injected at top of the column in the central part of the column and counter-current gas flow is applied using a diffuser at the bottom of the column. A precise description of the experimental set-up is given in Fourati et al. (2012). Adapted liquid flow distributors have been used in order to generate the non-uniform liquid flow distribution at the top of the packed bed and tomographic liquid hold-up (also named liquid saturation $\theta_L$) maps have been measured at different axial positions along the bed height. A sketch of the experimental set-up with the four axial positions, denoted $z_i$ ($i=1$ to 4) at which tomography measurements have been performed, is given in Fourati et al. (2012). The distances from the liquid inlet are $z_1=32$ cm, $z_2=48$ cm, $z_3=74$ cm and $z_4=110.5$ cm. Liquid hold-up measurements were carried out over a large range of experimental conditions: the liquid load being varied from 16 $m^3/m^2/h$ to 56 $m^3/m^2/h$ and the gas kinetic factor from 20% to 80% of its flooding value. As discussed in Fourati et al. (2012) tomography allows to measure liquid hold-up with an absolute error of 3%. Pressure drop measurements, reported and discussed in Fourati et al. (2012), are provided, when necessary, in the present discussion.

We also tested two couples of fluids: air–water or air–monoethanolamine with 30% mass fraction in water.

In the present study we discuss air–water experiments and focus on low liquid load ($q_L=16\ m^3/m^2/h$) and gas kinetic factors $F_S$ equal to 20% and 60% of the flooding condition $F_C$ as determined from experiments ($F_S=20\%F_C=0.74\ Pa^{0.5}$ and $F_S=60\%F_C=2.21\ Pa^{0.5}$).

Fig. 1 shows liquid retention maps obtained at the different axial positions along the bed for a liquid flow rate of $q_L=16\ m^3/m^2/h$ and a gas $F$-factor $F_S=\rho_G^{1/2}U_{GS}$ equal to 0.74 $Pa^{0.5}$ in case A and to 2.21 $Pa^{0.5}$ in case B. One observes that the liquid dispersion seems quite fast in the structured packing and that a homogeneous flow is almost achieved at position $z_4$ (1.1 m below liquid injection) whatever the gas flow rate. Positions $z_1$ and $z_2$ are located in the first packing element. This is the reason why, at these positions, liquid distribution remains aligned with the solid metal sheets of the packing for both cases. For downstream positions ($z_3$ and $z_4$), the liquid distribution is already isotropic. The liquid volume fraction still varies a lot at small scale, as liquid flows in films located along the solid matrix but the spreading of the liquid shows no significant heterogeneities at

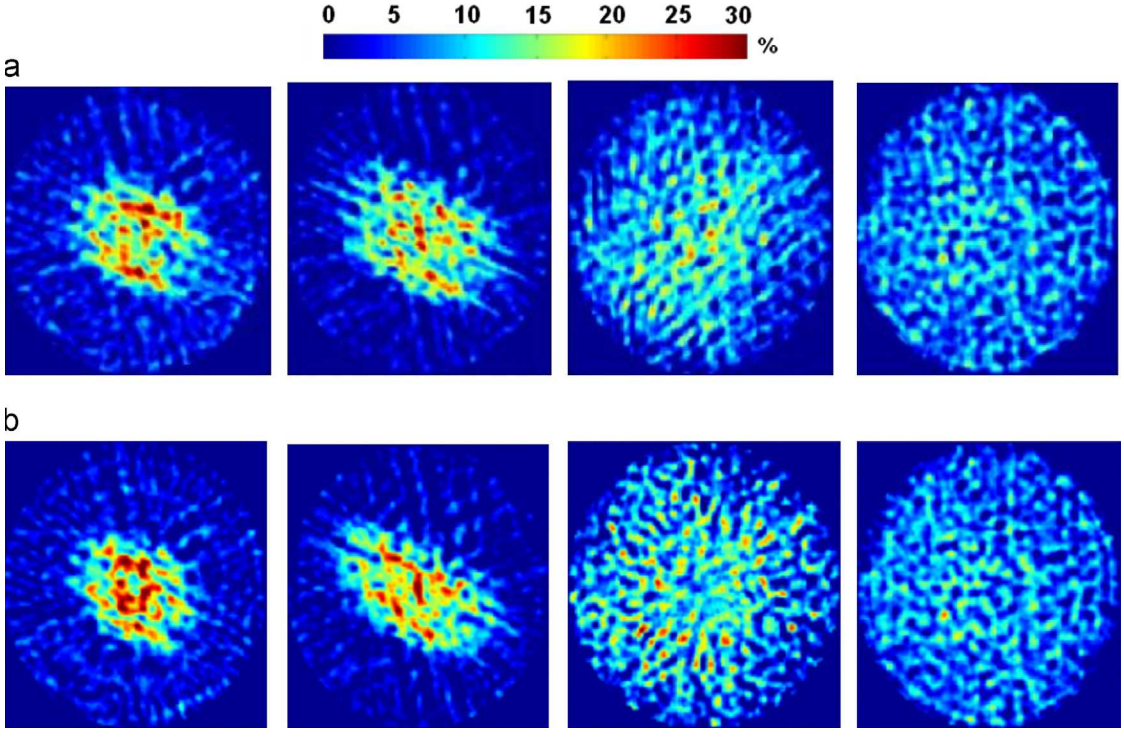


**Fig. 1.** Liquid hold-up maps obtained by tomography for two runs with air and water in Mellapak 250.X, $q_L=16\ m^3/m^2/h$, a/case (A) $F_S=0.74\ Pa^{0.5}$, b/case (B) $F_S=2.21\ Pa^{0.5}$. (Positions from left to right: $z_1$, $z_2$, $z_3$ and $z_4$).

large scale. We can thus consider a homogenized approach for modeling at large scale.

Liquid spread factors have also been determined from these maps in order to characterize liquid dispersion. The spread factor, $D_r$, is a length scale factor related to dispersion in a transport model for the liquid. It is introduced in a simple advection–diffusion transport equation for the liquid flow rate $q_L$ averaged at a meso-scale as discussed by Edwards et al. (1999) for structured packings. In cylindrical coordinates, this equation is written as follows:

$$\frac{\partial q_L}{\partial z} = D_r \frac{1}{r}\frac{\partial}{\partial r}\left(r\frac{\partial q_L}{\partial r}\right) \quad (1)$$

The local liquid flow rate $q_L$ is not measured directly. The liquid hold up being measured by tomography, we obtain $q_L$ by using an experimental correlation obtained in homogeneous flows that gives $\theta_L = k q_L^{0.4}$ (Eq. (6) in Fourati et al. (2012)). Then, the comparison between the experimental results and a theoretical solution of $q_L(z,r)$, considering the spreading of liquid from a point source within an infinite packed-bed, gives access to the spread factor (Fourati et al., 2012). We found that, changing the liquid and gas flow rates, the dispersion behavior remains identical whatever the flow conditions in the structured packing. For each run, we found a unique spread factor $D_r = 3.7$ mm. We discuss in part 4 how such a dispersion coefficient $D_r$, evaluated from Eq. (1), can be further used as a closure law in an Euler/Euler approach based on primary physical balances enabling accurate 3D simulations of complete columns.

## 3. Numerical model

We develop an Euler–Euler model solving local mass and momentum balances in gas and liquid phases to predict the hydrodynamics in packed columns. The transport equations deal with average quantities that are volume-averaged over a representative elementary volume $V$ with a length scale far smaller than the column size but large enough to give rise to well behaved averaged values.

The volume averaging procedure was well established by Whitaker and his collaborators in the framework of porous media (see as a starting point: Whitaker, 1973; Whitaker, 1986; and as a general reference: Whitaker, 1999). This averaging was also discussed by Liu (1999) and Liu and Masliyah (in Vafai, 2005) in order to prepare proposals for closure laws adapted to inertial two-phase flows in packings with high porosities. Several authors also discussed precisely the averaging for trickle-bed geometries taking into account or not partial wetting of the bed (Attou et al., 1999; Iliuta and Larachi, 2005). Averaging for periodic packings and monoliths was also discussed by Mewes et al. (1999).

In the present study, we consider isothermal and incompressible flows, where both phases are Newtonian, with no mass transfer at the gas–liquid interface and no chemical reaction.

### 3.1. Primary equations

#### 3.1.1. Geometric relations

The averaging procedure introduces the local volume fractions of each phases $\alpha_k$, and their saturations $\theta_k$. They are defined as $\alpha_k = V_k/V$ and $\theta_k = V_k/(V_G+V_L)$ where $V_k$ is the volume occupied by phase $k(=$G or L) and $V$ includes the volume of solid. Both quantities are related by $\alpha_k = \varepsilon\theta_k$ through the porosity defined as $\varepsilon = (V_G+V_L)/V$.

Due to the absence of overlapping of the phases, the geometric relation writes

$$\theta_G + \theta_L = 1 \quad (2)$$

#### 3.1.2. Mass balances

In each phase the mass balance is written:

$$\frac{\partial}{\partial t}(\varepsilon\theta_k\rho_k) + \vec{\nabla}.(\varepsilon\theta_k\rho_k\vec{U}_k) = 0 \quad k = \text{L, G} \quad (3)$$

where $\vec{U}_k$ is the intrinsic volume-average velocity of phase $k$ defined as $\vec{U}_k = 1/V_k \int_{V_k} \vec{u}_k dV$.

#### 3.1.3. Momentum balances

In each phase the momentum balance is written, assuming that capillary effects are negligible for Mellapack packing due to large dimensions of the elementary channels:

$$\frac{\partial}{\partial t}(\varepsilon\theta_k\rho_k\vec{U}_k) + \vec{\nabla}.(\varepsilon\theta_k\rho_k\vec{U}_k\vec{U}_k) = -\varepsilon\theta_k\vec{\nabla}P + \vec{\nabla}.(\varepsilon\overline{\overline{\tau_k}}) + \varepsilon\theta_k\rho_k\vec{g} + \varepsilon\vec{R}_{Ik} + \theta_k\vec{S}_{porous,k} + \vec{F}_{disp,k} \quad k = \text{L, G} \quad (4)$$

We thus define a unique average pressure, denoted $P$, for both phases. The first term in the right hand side (r.h.s.) of Eq. (4) is the pressure force, the second term introduces the average stress tensor $\overline{\overline{\tau_k}}$. It is a viscous term that is often negligible because it involves spatial derivatives of the average velocity which are always far smaller than the spatial derivatives of the velocity at the scale of the elementary channel of the packing. The shear stresses and pressure forces acting in the representative elementary volume either at the interfaces or at the walls lead to the average momentum transfer terms $\varepsilon\vec{R}_{Ik}$ and $\theta_k\vec{S}_{porous,k}$, respectively. Their modeling is described in the following paragraph. The last term, denoted $\vec{F}_{disp,k}$, is a dispersive term that has been added to model forces leading to mechanical dispersion. Its origin and modeling is discussed further.

The interfacial momentum balance is then written neglecting capillary forces as:

$$\vec{R}_{IG} + \vec{R}_{IL} = \vec{0} \quad (5)$$

The porosity that appears in mass and momentum balances is not a transported quantity. Its spatial distribution can be prescribed as resulting from the building of the packing. In the present work we choose a uniform porosity, $\varepsilon = 0.98$.

### 3.2. Closure laws

#### 3.2.1. Momentum transfers at the walls of the packing and at the gas–liquid interfaces

Recent proposals have been successfully tested to model the momentum transfers at the walls and at the gas–liquid interfaces in trickle-beds or structured packings (Holub et al., 1993; Attou et al., 1999; Iliuta et al., 2004; Lappalainen et al., 2009a).

#### 3.2.2. Momentum transfer at the walls

The proposed modelings for $\vec{S}_{porous,k}$ are issued from a generalized Ergun correlation primarily proposed for single-phase flows in packed beds (Ergun, 1952; Macdonald et al., 1979):

$$\vec{S}_{porous,k} = -\left(\mu_k\overline{\overline{D}}_k.\vec{U}_k + \frac{1}{2}\rho_k\|\vec{U}_k\|\overline{\overline{C}}_k.\vec{U}_k\right).$$

Reduced to its isotropic form this term writes:

$$\vec{S}_{porous,k} = -\left(\frac{\mu_k}{A_k}\vec{U}_k + \frac{1}{2}C_k\rho_k\|\vec{U}_k\|\vec{U}_k\right) \quad (6)$$

The resistance tensors $\overline{\overline{D}}_k$ and $\overline{\overline{C}}_k$ or their isotropic corresponding permeability $A_k$ and coefficient $C_k$ are modeled on a phenomenological basis to describe the effect, at a macroscale, of the complex geometry imposed by the solid matrix and of the flow regime at the microscale. The first term in Eq. (6) is dominant for viscous regimes, and the second one appears due to inertial effects. In single-phase flow ($SP$) and for the viscous regime,

Kozeny–Carman scaling law extends Darcy law by giving the permeability $A_k$ for complex or random porous geometries as a function of the averaged characteristic of the geometry. This law writes $A_{SP}=l^2\varepsilon^2/C_{CK}$ where $l$ is an appropriate length scale usually taken equal to the inverse of the volumetric surface area $a_g^{-1}$ and $C_{CK}$ is a constant generally equal to 5. This proposal gives reasonable permeabilities for random packings of spheres, periodic arrays of spheres or fractal porous media, but is not sufficient for multiscale geometries (Valdes-Parada et al., 2009).

Ergun proposal for single-phase flows introduces inertial effects appearing as the second term in Eq. (6) also named Forchheimer correction. For non negligible velocities, the dependence of $\vec{S}_{\text{porous},k}$ upon the square value of the velocity was theoretically demonstrated by Whitaker (1996) even if this was already well-known from experimental evidence. It is important to notice that this inertial effect is additional to the viscous one, and that it does not replace it. In fact, inertial effects are not associated to a laminar–turbulent transition in the flow at the pore scale as they appear in infinite straight pipes. This is clear as they appear for Reynolds numbers in the pores smaller than 100. They must be understood as supplementary form drag linked to additional spatial accelerations at the pore scale appearing with flow recirculations for example (as discussed by Prieur du Plessis, 1994). Following Ergun first proposal the coefficient $C_k$ is usually taken as proportional to $a_g/6\varepsilon^2$.

In two-phase flows, usually, to model each transfer term at the walls $\vec{S}_{\text{porous},k}$, permeabilities have been adapted. The permeabilities are linked to a hydraulic diameter at the microscale of the involved phase. They are thus related to the porosity $\varepsilon$, the effective area $a_g$ and the phase saturations $\theta_k$ (Holub et al., 1993; Iliuta et al., 2004). Another difficulty due to two-phase flow is to take into account the wetting of the solid surface in the models. A fractional wetted area $f_e$ is introduced to weight the momentum transfer terms. When $f_e=1$, at locations where gas and liquid phases co-exist, the liquid is assumed to wet totally the walls and there is no shear stress at the walls for the gas. Of course, in single-phase regions occupied by gas alone, the momentum transfer at the wall of the porous medium is retained for the gas phase. In order to simulate partial wetting ($f_e<1$), we have applied the general formulation of the model by Lappalainen et al. (2009a): the momentum transfer at the walls and at the interfaces are, respectively weighted by $f_e$, $(1-f_e)$ and $f_e$ for the liquid, for the gas and for the gas–liquid interface (see Eqs. (7)–(9) hereafter).

Iliuta et al. (2004) or Iliuta and Larachi (2005) have proposed closures specific for structured packing:

$$\vec{S}_{\text{porous},L}=-f_e\left(\frac{E_1}{36}\times\frac{a_g^2 f_e}{\varepsilon\theta_L^2}\mu_L+\frac{E_2}{6}\frac{a_g}{\theta_L}\rho_L\|\vec{U}_L\|\right)\vec{U}_L=-K_{LS}\vec{U}_L \tag{7}$$

$$\vec{S}_{\text{porous},G}=-(1-f_e)\left(\frac{E_1}{36}\times\frac{a_g^2}{\varepsilon}\mu_G+\frac{E_2}{6}a_g\rho_G\theta_G\|\vec{U}_G\|\right)\vec{U}_G=-K_{GS}\vec{U}_G \tag{8}$$

Both closure laws have similar mathematical forms with different hydraulic diameter: $6a_g^{-1}$ for the gas phase and $\theta_L/a_g$ for the liquid one, which is indeed representative of the liquid film thickness. In the present work we have retained the model of Iliuta and Larachi (2005) with their values of $E_1$ and $E_2$ (for Mellapak 250.X:$E_1=160$ and $E_2=0.16$). Strickly speaking, inside the parenthesis in Eq. (7) the wetting efficiency $f_e$ is approximated equal to 1. We just keep the multiplying factor $f_e$ in $\vec{S}_{\text{porous},L}$ and resp. $(1-f_e)$ in $\vec{S}_{\text{porous},G}$.

### 3.2.3. Momentum transfer at the gas–liquid interfaces

The general closure law adopted for the momentum transfer at the gas–liquid interfaces is similar to those at the walls. From Iliuta and Larachi (2005) we have:

$$\vec{R}_{IG}=-f_e\left(\frac{E_1}{36}\times\frac{a_g^2\theta_G}{\varepsilon^2(1-\theta_L/f_e)^2}\mu_G+\frac{E_2}{6}\frac{a_g{\theta_G}^2}{\varepsilon(1-\theta_L/f_e)^2}\rho_G\|\vec{U}_G-\vec{U}_L+\frac{\theta_L}{\theta_G}(1-\frac{1}{f_e})\vec{U}_L\|\right)\times\left(\vec{U}_G-\vec{U}_L+\frac{\theta_L}{\theta_G}(1-\frac{1}{f_e})\vec{U}_L\right) \tag{9-1}$$

When the order of magnitude of fractional wetted area $f_e$ is 1, and $\vec{U}_G-\vec{U}_L\gg\theta_L/\theta_G(1-1/f_e)\vec{U}$, as it is the case in the present experimental conditions (see discussion in Section 4), Eq. (9-1) may be simplified and gas–liquid interaction written as follows

$$\vec{R}_{IG}=-f_e\left(\frac{E_1}{36}\times\frac{a_g^2}{\varepsilon^2\theta_G}\mu_G+\frac{E_2}{6}\frac{a_g}{\varepsilon}\rho_G\|\vec{U}_G-\vec{U}_L\|\right)\times(\vec{U}_G-\vec{U}_L)=-K_{IG}(\vec{U}_G-\vec{U}_L) \tag{9-2}$$

### 3.2.4. Discussion

To our knowledge there are no theoretical derivations of permeability expressions in two-phase flows except for a set of parallel non-connected identical tubes in pure viscous laminar regime (Bacri et al., 1990). The present model (Eqs. (7)–(9-2)) is based on the idea that Ergun general correlation can be used to reproduce the momentum transfers at the walls or at the interfaces, provided pertinent velocity and permeability are chosen for each transfer term. The values of the factors $E_1$ and $E_2$ are also taken unchanged in $\vec{S}_{\text{porous},L}$, $\vec{S}_{\text{porous},G}$ and $\vec{R}_{IG}$. We would like to show, with a simple example, that such proposal is of course of great interest in the absence of theoretical derivation, but that it has to be taken with care.

Holub et al. (1993) and then Iliuta et al. (2000) developed semi-analytical models where the porous medium is divided in slits in which the two-phase film flow is modeled before applying slit to bed relations to obtain macroscopic models of $\vec{S}_{\text{porous},k}$ and $\vec{R}_{IG}$. Holub et al. (1993) developed a slit model for liquid films totally wetting the solid, while Iliuta et al. (2000) developed a double-slit method to take into account partial wetting. We retain their idea to analyze an ideal porous medium consisting in a set of parallel non-connected identical slits, but we follow, similarly to Bacri et al. (1990) an analytical approach based on Navier–Stokes resolution for steady, developed, laminar incompressible flow at the scale of the slit. This reduces the generality of the expected model, as inertial effects are not taken into account, but it allows discussing the origin of the closed terms. Our objectives are to discuss the meaning of the closure laws, the pertinence of the velocity and length scales adopted in these laws and the generality of the permeabilities adopted at least for the viscous resistances in two-phase flows.

Let us consider first the analytical solution of the flow between two fluids (subscripts 1 and 2) confined in a plane channel of width $h$ flowing along direction $x$ (co-currently or with a countercurrent configuration as shown in Fig. 2). Due to gravity or to inertia in the vertical case, phases are assumed to be separated so that the flow is associated to a wetting efficiency equal to 1/2. The averaged values of the velocities and of the widths of both phases are denoted $U_1$, $U_2$, $h_1$ and $h_2$. The signs of $U_1$and $U_2$ define co-current or counter-current flows. We can solve the Navier–Stokes equations in each phase which are coupled by the boundary condition at the fluid interface. The velocity components in $(x, y)$ plane are denoted $(u_k, v_k)$. Assuming a parallel flow, the continuity equations write:

$$v_k(y)=0\quad(k=1,2) \tag{D1}$$

Momentum balances reduce to: $\mu_k du_k/dy=K_k$ where the constant value

$$K_k=dP_k/dx-\rho_k g\sin(\theta)\quad(k=1,2) \tag{D2}$$

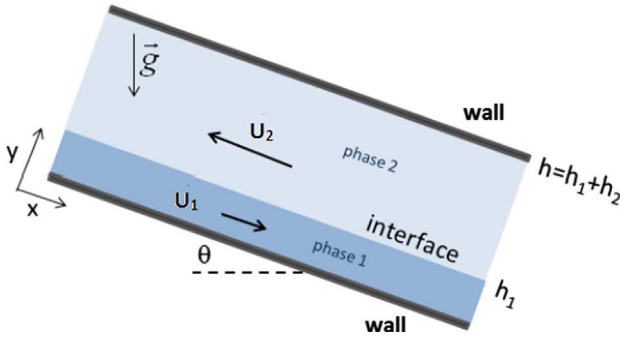


**Fig. 2.** Scheme of the two-phase flow in a slit.

with the following boundary conditions (BC):

(BC1) $u_1 = 0$ at $y=0$
(BC2) $u_1 = U_I$ at $y=h_1$
(BC3) $u_2 = 0$ at $y=h=h_1+h_2$
(BC4) $u_2 = U_I$ at $y=h_1$

where $h_1$ and $U_I$ the position and velocity of the interface are unknown.

The velocity profiles $u_k(y)$ can then be obtained and expressed using $K_k$ $U_I$, $h$ and $h_1$. By integrating these velocity profiles in the $y$ direction, one can relate the average velocity of each flow to the interface velocity and pressure gradient:

$$U_k = \frac{U_I}{2} - \frac{K_k h_k^{\,2}}{12\mu_k} \quad (k=1,2) \tag{D3}$$

The shear stresses at the walls and on each side of the interface can also be expressed as:

$$\tau_{w1} = -\mu_1 \frac{dU_1}{dy}\Big)_{y=0} = -\mu_1\left(\frac{U_I}{h_1} - \frac{K_1 h_1}{2\mu_1}\right) = -\frac{\mu_1}{h_1}(6U_1 - 2U_I) \tag{D4}$$

$$\tau_{w2} = \mu_2 \frac{dU_2}{dy}\Big)_{y=h} = \frac{\mu_2}{h_2}(2U_I - 6U_2) \tag{D5}$$

$$\tau_{I1} = \mu_1 \frac{dU_1}{dy}\Big)_{y=h_1} = \mu_1\left(\frac{U_I}{h_1} + \frac{K_1 h_1}{2\mu_1}\right) = \frac{\mu_1}{h_1}(4U_I - 6U_1) \tag{D6}$$

$$\tau_{I2} = -\mu_2 \frac{dU_2}{dy}\Big)_{y=h_1} = \frac{\mu_2}{h_2}(4U_I - 6U_2) \tag{D7}$$

The last boundary condition that must be verified is the continuity of the shear stress at the interface ((BC5) $\tau_{I1} + \tau_{I2} = 0$). This leads to:

$$U_I = \frac{3}{2}\left(\frac{\mu_1/h_1 U_1 + \mu_2/h_2 U_2}{\mu_1/h_1 + \mu_2/h_2}\right) \tag{D8}$$

The prediction of the position of the interface $h_1$ for the fully developed flow could be achieved by equating the pressure gradients in each fluid. For our present purpose we just rewrite the shear stresses using the known value of $U_I$ (given by Eq. (D8)):

$$\tau_{I2} = 6\frac{(U_1 - U_2)}{h_1/\mu_1 + h_2/\mu_2} \tag{D9}$$

$$\tau_{w1} = -3\frac{\mu_1}{h_1}U_1 - 3\frac{(U_1 - U_2)}{h_1/\mu_1 + h_2/\mu_2} \tag{D10}$$

$$\tau_{w2} = -3\frac{\mu_2}{h_2}U_2 + 3\frac{(U_1 - U_2)}{h_1/\mu_1 + h_2/\mu_2} \tag{D11}$$

At the slit scale the momentum equations averaged across the width of each phase then write:

$$0 = -\theta_{ks}\frac{dP}{dx} + \theta_{ks}\rho_k g\sin(\theta) + F_{Ik} + F_{wk} \quad (k=1,2) \tag{D12}$$

with $\theta_{ks} = h_k/h$ the saturation at the slit scale, and $F_{Ik} = \tau_{Ik}/h$, $F_{w1} = \tau_{w1}/h$.

We now apply an elementary homogenization method to obtain the macroscopic equations valid for the porous medium from the local solution in a slit. We consider that the porous geometry consists in an array of parallel slits. The variables describing the slit geometry are related by slit-to-bed relations to the macroscopic properties of the porous medium. These relations express that the saturation of each phase and the volume fraction of the solid, as well as the intrinsic velocity or pressure gradient are the same at the macroscopic scale and in the representative slit. We can thus write in a macroscopic volume-average sense:

$$0 = -\varepsilon\theta_{ks}\frac{dP}{dx} + \varepsilon\theta_{ks}\rho_k g\sin(\theta) + \varepsilon F_{Ik} + \varepsilon F_{wk} \quad (k=1,2) \tag{D13}$$

For a homogeneous flow, an identification of (D13) with Eq. (4) leads to the following relations where we used the analytical solution to express the shear stress terms:

$$\varepsilon R_{Ikx} + \theta_k S_{\text{porous},kx} = +\varepsilon F_{Ik} + \varepsilon F_{wk} = \frac{6\varepsilon}{h^2}(-1)^k \frac{(U_1 - U_2)}{\theta_1/\mu_1 + \theta_2/\mu_2} - 3\varepsilon\frac{\mu_k}{h^2\theta_k}U_k + \frac{3\varepsilon}{h^2}(-1)^k\frac{(U_1 - U_2)}{\theta_1/\mu_1 + \theta_2/\mu_2} \tag{D14}$$

It must be recalled that the first term on the r.h.s. is equal to interfacial shear stress term $\varepsilon R_{Ikx}$ and that the second and third terms are equal to the shear at the wall term $\theta_k S_{\text{porous},kx}$.

We must notice that, if the velocity that appears in the interfacial shear stress $F_{Ik}$ is the relative velocity between both phases (see also Eq. (D9)), the general expression for $F_{wk}$, the shear stress of phase $k$ at the wall, is not simply related to the average velocity of phase $k$ (see also Eqs. (D10) and (D11)): the relative velocity also appears in $F_{wk}$. This is a deviation as compared to common macro-scale closure laws proposed in the literature that we discuss hereafter.

Eq. (D9) also shows that interfacial shear stress is symmetrically written according to the physical properties of both phases in the general case. Closure laws proposed for gas–liquid flows in the literature do not retain such symmetry (Holub et al., 1993, Iliuta et al., 2004). In the present study, the viscous part of the closure law we adopted (Eq. (9–2)) reduces to:

$$\vec{R}_{\text{IGV}} = -f_e\left(\frac{E_1}{36}\times\frac{a_g^2}{\varepsilon^2\theta_G}\mu_G\right)(\vec{U}_G - \vec{U}_L) = -K_{\text{IGV}}(\vec{U}_G - \vec{U}_L) \tag{D15}$$

Linear dependency of the closure law with the relative velocity is in agreement with the analytical solution $R_{Ikx}$ given in Eq. (D14), but the permeability associated to interfacial momentum transfer is written only with the physical properties of the gas. This simplification is, however, in agreement with the analytical solution just because condition $h_1/\mu_1 \ll h_2/\mu_2$ is easily verified for thin liquid films sheared by gas flow (indexes 1 and 2 being associated with liquid and gas). We may therefore retain that the analytical solution shows that it may be necessary to introduce the physical properties of both phases in the closure laws for applications where such condition would not be verified (in liquid—liquid systems for example).

The viscous parts of the porous resistances associated to momentum transfer at the walls as given in the closure laws Eqs. (7) and (8) write:

$$\vec{S}_{\text{porous,LV}} = -f_e\left(\frac{E_1}{36}\times\frac{a_g^2 f_e}{\varepsilon\theta_L^2}\mu_L\right)\vec{U}_L = -K_{\text{LSV}}\vec{U}_L \tag{D16}$$

$$\vec{S}_{\text{porous,GV}} = -(1-f_e)\left(\frac{E_1}{36}\times\frac{a_g^2}{\varepsilon}\mu_G\right)\vec{U}_G = -K_{GSV}\vec{U}_G \quad \text{(D17)}$$

Comparing (D16) and (D17) with (D14) make noticeable differences appear. The analytical solution gives momentum transfer terms $S_{\text{porous},kx}$ that involve both the velocity of phase $k$ and the relative velocity, while closure laws (D16) and (D17) involve only the velocity of phase $k$. Also, physical properties of both phases appear in the relations giving $S_{\text{porous},kx}$, which is not the case for the closure laws. Models adopted in the literature for gas–liquid flows are correct, but as shown by this discussion, they are still a particular case. In fact, assuming $h_1/\mu_1 << h_2/\mu_2$ (or equivalently in gas–liquid flows $\theta_L/\mu_L << \theta_G/\mu_G$), it is possible to write from (D14):

$$S_{\text{porous,Lx}} = -3\varepsilon\frac{\mu_L}{h^2\theta_L^2}U_L - 3\varepsilon\frac{\mu_G}{h^2\theta_L\theta_G}(U_L-U_G)$$

and

$$S_{\text{porous,Lx}} \approx -3\varepsilon\frac{\mu_L}{h^2\theta_L^2}U_L \quad \text{(D18)}$$

Similarly for the gas phase, the assumption leads to:

$$S_{\text{porous,Gx}} = -3\varepsilon\frac{\mu_G}{h^2\theta_G^2}U_G + 3\varepsilon\frac{\mu_G}{h^2\theta_G^2}(U_L-U_G)$$

which reduces to:

$$S_{\text{porous,Gx}} \approx -3\varepsilon\frac{\mu_G}{h^2\theta_G^2}U_G \quad \text{(D19.a)}$$

for negligible relative velocity, or to:

$$S_{\text{porous,Gx}} \approx -6\varepsilon\frac{\mu_G}{h^2\theta_G^2}U_G \quad \text{(D19.b)}$$

when $U_G \gg U_L$, which is the case in carbon capture problems.

Eqs. (D18), (D19.a) and (D19.b) confirm that the usual closure laws adopted for momentum transfer at the wall for gas–liquid flows, assuming linear dependency upon the velocity of phase $k$, are valid in packings, which was expected from operational knowledge reported in the literature. But the analysis allows to precise that one should be careful to extend such closure laws to cases where the given assumptions would not be verified.

Finally, we can compare the viscous resistances for gas–liquid flows in structured packing either obtained from the analytical solution (Eqs. (D14), (D18) and (D19.b)) or from closure laws (Eqs. (D15), (D16) and (D17)) using, for a porous geometry consisting in an array of parallel slits, the relation $a_g = 2\varepsilon/h$, a fractional wetted area $f_e$ equal to ½ and $E_1 = 160$.

We may therefore compare:

$$K_{IGV} = \frac{6\mu_G}{h^2\theta_G}, \quad K_{LSV} \approx 3\varepsilon\frac{\mu_L}{h^2\theta_L^2} \quad \text{and} \quad K_{GSV} \approx 6\varepsilon\frac{\mu_G}{h^2\theta_G^2}$$

with the relations:

$$K_{IGV} = f_e\left(\frac{E_1}{36}\times\frac{a_g^2}{\varepsilon^2\theta_G}\mu_G\right) \approx 8.9\frac{\mu_G}{h^2\theta_G},$$

$$K_{LSV} = f_e\left(\frac{E_1}{36}\times\frac{a_g^2 f_e}{\varepsilon\theta_L^2}\mu_L\right) \approx 4.45\frac{\varepsilon\mu_L}{h^2\theta_L^2} \quad \text{and}$$

$$K_{GSV} = (1-f_e)\left(\frac{E_1}{36}\times\frac{a_g^2}{\varepsilon}\mu_G\right) \approx 8.9\frac{\varepsilon\mu_G}{h^2}.$$

For porosity and gas volume fraction around 1, the orders of magnitude of ‖ both expressions of the various resistances are in agreement even if differences still remain. It must be nevertheless noticed that the scaling law of $K_{GSV}$ are different concerning $\theta_G$ contribution. For Mellapak 250.X this is not so important because $\theta_G$ is around unity, but revising the scaling laws could be interesting for other packing conditions. As a conclusion on the discussion about momentum transfer modeling we can say that theoretical models in elementary configurations, as proposed here, can help discussing the validity of efficient semi-empirical models as proposed in Eq. (7) to (9-2) which have been widely tested and prove to be predictive.

### 3.2.5. Dispersion term

In two-phase flows through porous media, dispersion terms appear due to volume averaging in the equations of momentum. Two distinct elementary mechanisms lead to momentum dispersion. The first one is the difference of pressures across the fluid interface due to capillarity: it leads to the macroscopic effect called *capillary dispersion*. The second one is the complex advection of momentum by the fluid at the pore scale. Local velocities of the phases are in general different from the volume-averaged velocities, and for inertial flows, when these deviations are correlated at the macroscopic scale, this leads to *mechanical dispersion*. In fact, the volume averaging of the non linear terms in the local momentum equation introduces in the macroscopic equation the divergence of the velocity deviation correlation tensor (Whitaker, 1973) which can be understood as an analogous to the Reynolds stress tensor in turbulence (Grosser et al., 1988).

### 3.2.6. Capillary dispersion models

To take into account capillary dispersion, the first way could be to keep two pressures (one for each phase) in the macroscopic equations (Whitaker, 1986). But most often two-fluid Eulerian models use a unique pressure identified as the pressure in the gas phase and introduce a closure law for the capillary pressure $P_c = P_G - P_L$. In such approach Eq. (4) for the liquid phase should include a dispersion term $\vec{F}_{disp,L,c} = \varepsilon P_c\vec{\nabla}\theta_L$ such as proposed by Attou and Ferschneider (2000), Boyer et al. (2005) or Jiang et al. (2002). The capillary pressure, which is related to interface curvature through Laplace law, is then given as a function of the liquid volume fraction at the macro-scale (Attou and Ferschneider, 2000; Boyer et al., 2005). For general porous media or for trickle-beds the closure law for $P_c(\theta_L)$ is either obtained from experimental tests leading to a correlation introducing the Leverett function, or obtained from geometrical considerations about the gas–liquid interface curvature at the pore scale (Attou and Ferschneider, 2000; Jiang et al., 2002; Lappalainen et al., 2009b). Lappalainen et al. (2009b) used a different model for capillary dispersion. They wrote in the momentum equation of the liquid phase: $\vec{F}_{\text{disp,L,c}} = \varepsilon\theta_L\vec{\nabla}P_c$ which is not equivalent to the aforementioned term. Careful discussion of the modeling of this capillary dispersion term would be required to see the validity of such proposal.

In our study of structured packings, we do not take into account the capillary dispersion. This approximation is justified because the size of the packing elements is quite large so that we can argue that capillary pressure vanishes. Even if the curvature of the interface varies a lot at the pore scale we can give arguments that lead to neglect capillary pressure in our study. It is interesting to notice from Whitaker (1986) (Eq. 3.14) that volume-averaged pressures of each phases $P_L$ and $P_G$ are not simply related to the volume-averaged value $H$ of the interface curvature. The complete momentum interfacial relation includes normal viscous forces. The relation between the orders of magnitude then writes:

$$P_G - P_L = 2\sigma H + o\left(\max_k\left(\frac{\mu_k\|\vec{U}_k\|}{l_k}\right)\right)$$

where $l_k$ is the size of phase $k$ at the pore scale. In our flow conditions the second term on the r.h.s. is due to the liquid phase.

Estimating $l_k$ as the liquid film width $e$, and $e$ as $\theta_L/a_g$, we find that this second term is around 0.5 Pa which is negligible as compared to Laplace term: taking the averaged value of $H$ equal to the inverse of the hydraulic diameter ($4\varepsilon/a_g$), we find in fact that $2\sigma H$ is about 6 Pa. The order of magnitude of the ratio of the capillary dispersion term to the pressure gradient term is thus $o(\|\vec{F}_{disp,L,c}\|/\|\varepsilon\theta_L\vec{\nabla}P_L\|) = o(P_c\|\vec{\nabla}\theta_L\|/\theta_L\|\vec{\nabla}P_L\|) \approx 2\sigma H/D_c/\|\vec{\nabla}P_L\|_{exp}$ with $D_c$ the column diameter and $\|\vec{\nabla}P_L\|_{exp}$ the pressure drop which order of magnitude is 100 Pa/m (Table 2). This ratio being about 0.15 the capillary pressure can be neglected.

### 3.2.7. Mechanical dispersion

Most theoretical analysis of flows in porous media are applied to single-phase flows in saturated viscous regimes with linear momentum equation at the pore scale so that there is no momentum dispersion. In such case, dispersion only appears in volume-averaged equations for the scalar transport due to the presence of advection and to specific surface integrals at the boundaries of the phase (Quintard and Whitaker, 1993). This may be the reason why existing models about dispersion in porous media have been mainly developed for scalar transport (Brenner, 1980; Carbonell and Whitaker, 1983; Eidsath et al., 1983; Liu and Masliyah in Vafai (2005)).

In two-phase flows through packings, inertia, interphase interactions and solid-phase interactions must be retained in volume averaged equations. In order to build such a system of volume averaged equations also able to reproduce dispersion, Liu (1999) proposed a volume-averaged approach including tortuosity effect and specific volume averaging rules. This approach introduces unclosed dispersion terms in mass and momentum equations. Liu and Long (2000) discussed a simplified version of the model for which they proposed semi-empirical closure laws. The assumptions of isotropic porous medium and of total wetting were introduced, but the generality of their proposal is unclear. It consists in adding in the momentum equation of the liquid phase a dispersive force $\vec{F}_{disp,L,1} = \vec{\nabla}.(\varepsilon\rho_L\overline{\overline{K_L}}.\vec{\nabla}(\theta_L\vec{U}_L/\tau_L))$ originating from the interaction of the liquid and the solid matrix, and in each momentum equation another dispersive force originating from interactions of both phases which writes for the gas phase $\vec{F}_{disp,lG} = \vec{\nabla}.(\varepsilon\rho_G\overline{\overline{K}}_{lG*}.\vec{\nabla}(\vec{U}_G/\tau_G - \theta_L\vec{U}_L/\tau_L\theta_L))$ and $-\vec{F}_{disp,lG}$ for the liquid. In these models $\tau_k$ are the tortuosities of the phases, $\overline{\overline{K}}_L$ and $\overline{\overline{K}}_{lG*}$ the dispersion tensors modeled from the analysis of passive scalar dispersion results.

One can find in the chemical engineering literature several other semi-empirical proposals to model the mechanical dispersion forcing terms $\vec{F}_{disp,k}$ governing liquid spreading. But these models are scarcely described and have most often no definitive theoretical basis except that their form is adequate to introduce dispersion. Moreover, to our knowledge, the only closure to have been tested with a comparison between numerical simulations and experimental results is the one of Lappalainen et al. (2009b, 2011). Mewes et al. (1999) introduced a general form able to generate an anisotropic dispersion term in the momentum equation of the liquid phase. It would write in our system of notations: $\vec{F}_{disp,L} = \overline{\overline{\xi}}.(\overline{\overline{S}} \times (\varepsilon\theta_L\vec{U}_L))$ where $\overline{\overline{\xi}}$ is a resistance tensor associated to shear stress at the walls that takes the simplified form $\overline{\overline{\xi}} = -K_{LS}/\varepsilon\overline{\overline{I}}_d$ for our isotropic model, and $\overline{\overline{S}}$ is a spreading tensor for which no closure law is proposed by the authors.

The discrepancy between the general models for mechanical dispersion proposed by Liu and Long (2000), Mewes et al. (1999) and Lappalainen et al. (2009a, 2011) shows that fundamental work is required to deduce dispersion terms from volume averaging of local balances. In the present work, we have retained the model tested by Lappalainen et al. (2009b, 2011). It consists in adding in the momentum equations of both phases the following terms:

$$\vec{F}_{disp,L} = \theta_L K_{LS}\vec{U}_{D,L} - \varepsilon K_{lG}(\vec{U}_{D,G} - \vec{U}_{D,L}) \tag{10}$$

$$\vec{F}_{disp,G} = \theta_G K_{GS}\vec{U}_{D,G} + \varepsilon K_{lG}(\vec{U}_{D,G} - \vec{U}_{D,L}) \tag{11}$$

where $\vec{U}_{D,G} = (-S\|\vec{U}'_G\|/\alpha_G)\vec{\nabla}\alpha_G$ and $\vec{U}_{D,L} = (-S\|\vec{U}_L\|/\alpha_L)\vec{\nabla}\alpha_L$ are drift velocities and $\vec{U}'_G = \vec{U}_G/\alpha_G$, $S$ is a spread factor whose dimension is length. Lappalainen et al. (2009a) identified the present spread factor with the one obtained from liquid flow rate distributions interpreted with a convection–diffusion equation of $q_L$ as written in part 2 of the present paper. We discuss briefly hereafter the physics underlying the validity of such assumption. The proposal of Lappalainen et al. (2009a) also assumes isotropic dispersion, and dispersion driving terms for both liquid and gas. In our flow regime, with high porosity and very thin liquid films, an order of magnitude study shows that the most important term ensuring liquid dispersion is $\vec{F}_{disp,L} = \theta_L K_{LS}\vec{U}_{D,L}$ which was indeed verified with numerical tests.

### 3.2.8. Discussion

It is important to notice that a spreading coefficient, S, appears in this model. It is possible to relate this spreading coefficient with the spreading factor, $D_r$, measured from the experiments assuming a convection–diffusion transport equation for the mass flow rate of the liquid as we did in part 2. This can be done if we assume that the dominant terms in the horizontal momentum balance for the liquid phase (Eq. 4) are related to shear stress at the walls and to dispersive term:

$$(\theta_k\vec{S}_{porous,L} + \vec{F}_{disp,L}).\vec{e}_h = 0 \tag{12}$$

where $\vec{e}_h$ is the horizontal unit vector. In cylindrical coordinates, with $\vec{e}_h = \vec{e}_r$, the momentum balance then writes: $-K_{LS}\theta_L U_{Lr} - K_{LS}S\|\vec{U}_L\|\partial\theta_L/\partial r = 0$ that is $\theta_L U_{Lr} = -S\|\vec{U}_L\|\partial\theta_L/\partial r$

This is equivalent to neglect accelerations, pressure gradients and gas–liquid interactions in the horizontal direction. This equilibrium leads to identify the horizontal average and drift liquid velocities in the mass balance of the liquid. For steady state flow, the mass balance writes:

$$\frac{\partial\theta_L U_{Lz}}{\partial z} + \frac{1}{r}\frac{\partial}{\partial r}\left(-rS\|\vec{U}_L\|\frac{\partial\theta_L}{\partial r}\right) = 0$$

From the mass balance in the liquid phase, assuming moreover that $U_{Lz} \approx \|\vec{U}_L\|$ is nearly uniform, one can thus obtain the modeled convection-diffusion transport equation for the liquid flow rate $q_L = \theta_L U_{Lz}$:

$$\frac{\partial\theta_L U_{Lz}}{\partial z} \approx S\frac{1}{r}\frac{\partial}{\partial r}\left(r\frac{\partial\theta_L U_{Lz}}{\partial r}\right) \tag{13}$$

Under the assumption of the previous peculiar momentum equilibrium and of uniform distribution of the liquid velocity, it is therefore possible to identify the spread factor determined from our global analysis of the experimental distribution of liquid flow rate ($D_r$) with the spread factor of the model ($S$) used by Lappalainen et al. (2009a). This identification is basically the one made by Lappalainen et al. (2009a). However, although it can be used as a first approximation, one could expect simulation results will not be totally satisfactory since derivatives of $\|\vec{U}_L\|$ in the radial direction are important in the case of a point-source liquid injection. Determination and discussion of best ratio $S/D_r$ will be provided later in this paper in the light of simulation results.

*3.2.9. Fractional wetting area*

For structured packings, the effective specific area of the solid may be lower than the geometric one which indicates partial wetting. Several studies found in literature focused on the ratio between effective surface area (equivalent here to wetted area) and the geometric one using mainly chemical methods. Effective packing specific area and then wetting factor is found to vary with liquid and gas flow rates as well as liquid surface tension. According to Olujic et al. (1999), both increased liquid load and low surface tension encourage a more important wetting of the packing surface. Weimer and Schaber (1996) (in Olujic et al., 1999) measured effective surface areas for metal Mellapak 250.Y in the range of 85–95% of the nominal surface area for liquid loads ranging from 15 $m^3/m^2/h$ to 30 $m^3/m^2/h$. This result of an interfacial area close to $a_g$ has been recently confirmed by the experiments performed by Tsai et al. (2011) on both Mellapak 250.X and Y.

Since we are dealing with Mellapak 250.X ($a_g = 250\ m^2/m^3$) in this work, the fractional wetted area $f_e$ is given by the correlation of Brunazzi and Paglianti (1997) developed for Mellapack packings. It is written as:

$$f_e = \frac{\sin(\theta)}{a_g} \times \theta_L^{1.5} \times \left(\frac{\rho_L \times g}{3 \times \mu_L \times U_{LS}}\right)^{0.5}$$

where $\theta$ refers to the corrugation angle of the packing (channel flow angle from horizontal equal to 60° in the case of Mellapak 250.X) and $U_{LS}$ to the superficial velocity of the liquid defined as follows: $U_{LS} = \varepsilon\theta_L \| \vec{U}_L \|$.

## 4. Discussion: Comparison between numerical simulations and experimental results

We have performed 2D axi-symmetric numerical simulations using the numerical code Fluent (version 13) with a pressure based unsteady state solver which appeared to be necessary to avoid numerical divergence. We developed original *user defined functions* for the porous resistances, for the interfacial transfer term and for the dispersive term. The interfacial transfer was implemented through a modification of the drag in a *define exchange properties* function. Resistances and dispersive terms were implemented as source terms using *define properties* functions. The total flow rates are $q_L = 16\ m^3/m^2/h$ for the liquid, and $F_S = 31.5\% F_C = 1.16\ Pa^{0.5}$ or $F_S = 60\% F_C = 2.21\ Pa^{0.5}$ for the gas. The geometry is adapted to simulate the column where experiments were performed that is described in details in Fourati et al. (2012). The domain for the calculations has a radius equal to 0.2 m, and a height equal to 0.76 m to simulate the part of the real column between liquid injection and the first three layers of structured packing. As shown in Fig. 3, we inject the liquid at the top of the column through a central part of radius $R_{injL} = 12$ mm. At the inlet, the liquid volume fraction is necessarily set equal to 1, and its velocity set to 1.19 m/s to ensure a flow rate equal to the experimental one. Physical gas inlet is at the bottom of the column; however, in order to facilitate counter-current calculations, it appeared that the best way was to fix at the residual part of the top of the column a boundary condition of gas inlet (with a negative velocity along the normal direction of the domain). The velocities of gas are set equal to 1.052 m/s and 2 m/s, respectively for both simulated cases. The bottom of the column is then defined as a pressure outlet where gas and liquid can, respectively freely go out of the domain, the gas being also able to re-enter the domain. The domain is also limited by the axis and by a symmetry boundary. The domain of calculation is divided into three parts, the packed bed of height 0.66 m with porous resistances and an upper and a lower part of total height 0.1 m with no porous resistance. They correspond to the regions empty of packing in the experimental setup present upstream and downstream the packed bed, respectively. The mesh grid has a size of 15,224 nodes with refined grid near the wall and in the central region of the liquid jet. In the radial direction, cell mean size is 0.5 mm in the liquid injection zone and 3 mm elsewhere with bell shaped sequence. In the axial direction, cell size is set to 5 mm. Second order upwind discretization schemes were used and the time step was about $10^{-4}$ s in order to ensure numerical convergence.

The simulated cases are described in Table 1. We have performed a simulation (case a) without any dispersion term and four others denoted cases b to e considering the dispersion term $\vec{F}_{disp,k}$ proposed by Lappalainen et al. (2009b, 2011). In three cases we considered a spread factor $S$ equal to $D_r = 3.7$ mm as measured in the experiments. In the case denoted e, we considered a spread factor $S$ equal to $2D_r = 7.4$ mm.

In cases a, b and d, the fractional wetted area was taken equal to 1 as a first approximation. It is thus assumed that, at the local scale, when both phases are present, the packing surface is totally covered by a continuous liquid film. One should notice at this point that the references considered in Section 3 analyzing partial wetting deal with homogeneous flows which is not the case for the present experiments and simulations. In fact, calculation of the superficial liquid velocity based on the injection surface leads to relatively important liquid loads so that we could consider, based on the upper bibliographic results, that total wetting is obtained in the limited region where liquid flows. However, in order to test sensitivity of results to partial wetting, we performed a simulation (case c) considering variable wetting factor based on correlation proposed by Brunazzi and Paglianti (1997).

**Table 1**
Simulated cases.

| Cases | Wetting factor $f_e$ | Spread factor | $q_L(m^3/m^2/h)$ | $F_S\ (Pa^{0.5})$ |
|---|---|---|---|---|
| a | 1 | No dispersion force | 16 | 1.16 |
| b | 1 | $S = D_r$ | 16 | 1.16 |
| c | Brunazzi and Paglianti (1997) | $S = D_r$ | 16 | 1.16 |
| d | 1 | $S = D_r$ | 16 | 2.21 |
| e | 1 | $S = 2\ D_r$ | 16 | 1.16 |

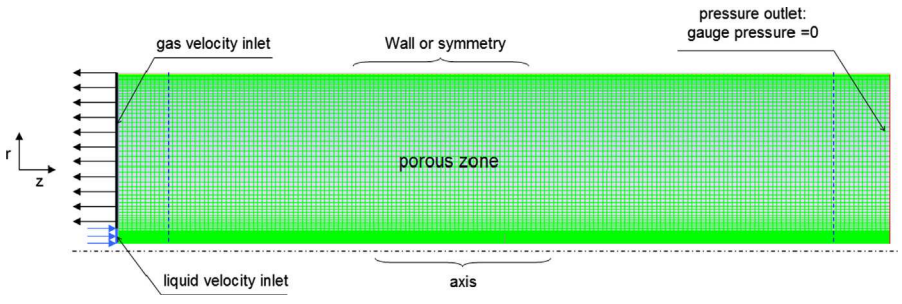


**Fig. 3.** Mesh and boundary conditions. (The porous zone is in between both blue dashed lines). (For interpretation of the references to color in this figure legend, the reader is referred to the web version of this article.)

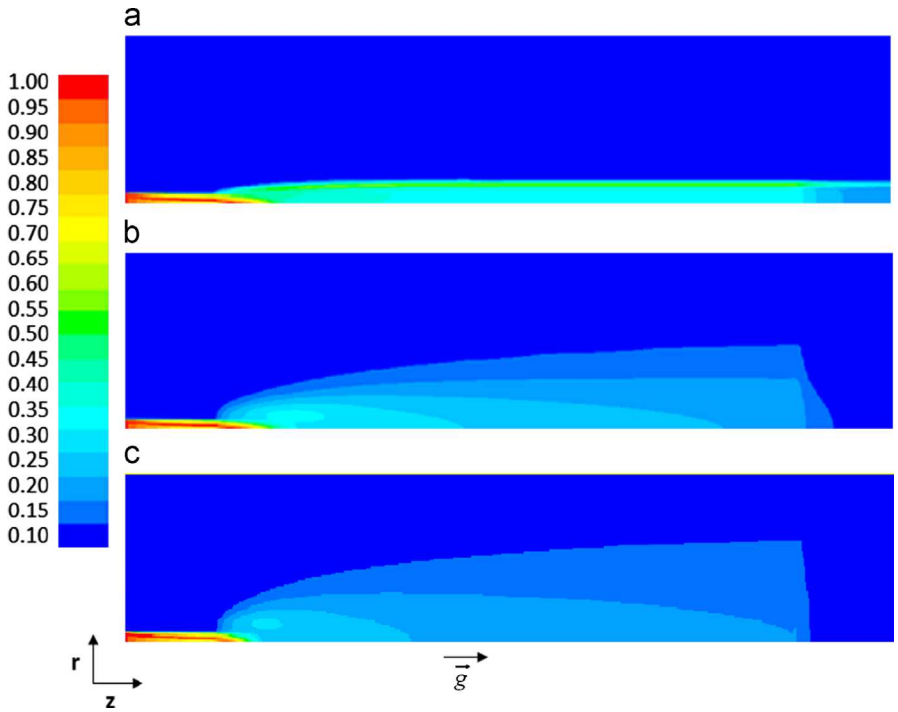


**Fig. 4.** Spatial distribution of liquid volume saturation $\theta_L$. ($q_L$=16 m$^3$/m$^2$/h, $F_S$=31.5%$F_C$), a/case a, $S$=0; b/case b, $S$=$D_r$,; c/case e, $S$=2$D_r$.

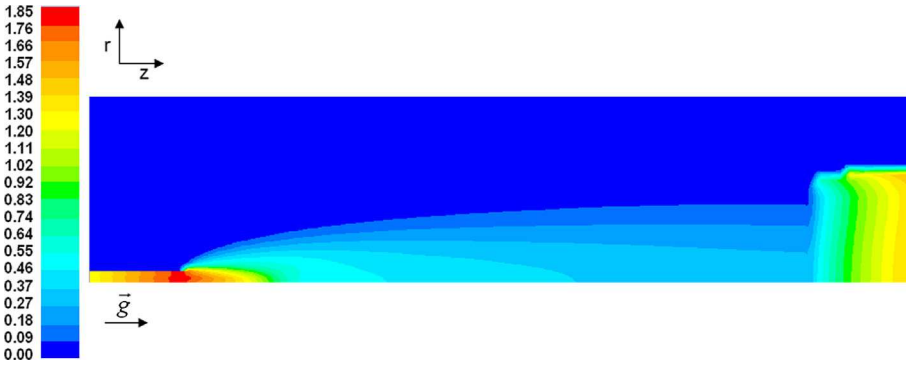


**Fig. 5.** Contours of liquid velocity magnitude (in m/s). ($q_L$=16 m$^3$/m$^2$/h, $F_S$=31.5%$F_C$), case b in Table 1.

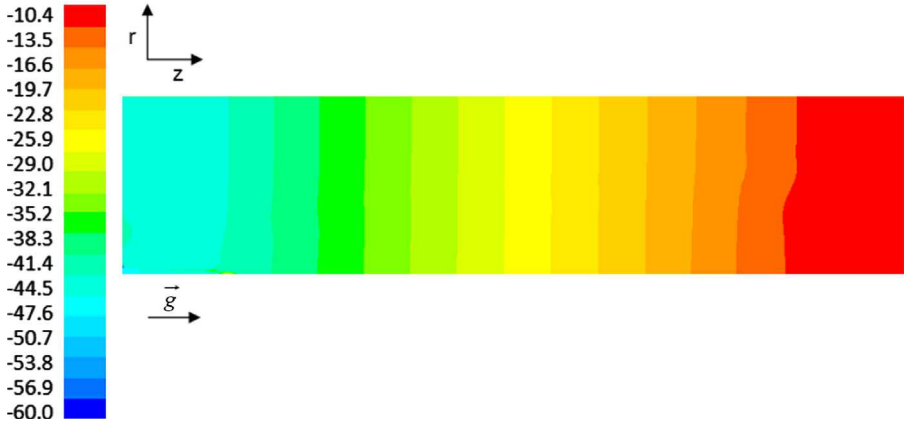


**Fig. 6.** Pressure field (Pa). ($q_L$=16 m$^3$/m$^2$/h, $F_S$=31.5%$F_C$), case b in Table 1.

Fig. 4 shows the liquid volume fraction contour maps. From the comparison of the cases without or with a dispersion model, one observes that it is essential to use such a model for dispersion to ensure radial spreading of the liquid. Indeed, case a (without dispersion model) provides a very narrow spatial distribution of liquid with an important overconcentration of liquid at its border

that could be the memory of the liquid impact on the porous zone. On the contrary, when a model for dispersion is used (case b and e), both the liquid saturation (Fig. 4) and the liquid velocity (Fig. 5) spread in the radial direction. The liquid decelerates in the porous medium due to shear stresses at the walls and to interfacial shear stress applied by the countercurrent gas flow. The pressure distribution is not very sensitive to the distribution of liquid. Fig. 6 shows a dominant axial evolution of the pressure as if the liquid inlet conditions were homogeneous. This has already been observed in the experiments were pressure drop was similar for homogeneous injection or central injection of liquid. It may be explained by the fact that liquid films remain very thin in our flow conditions. The overall predicted pressure gradients are summarized in Table 2. In all cases, values of pressure drop are globally in good agreement with the ones measured in the experimental set-up. This was expected since the model of porous resistance that we took proved to be representative for Mellapak 250.X (Iliuta et al., 2004).

In the non porous zone in the lower part of the simulated column, boundary conditions influence liquid velocity as well as static pressure distributions. Their impact on gas velocity will be discussed further.

On Fig. 7a we have reported the radial liquid saturation profiles obtained from gamma-ray tomography at three axial positions of measurement $z_1$, $z_2$ and $z_3$ (Fourati et al., 2012), and the numerical results at the same positions for $S=D_r$ and $S=2D_r$. The experimental values were measured at a different gas flow rate ($F_S=0.74\ \mathrm{Pa}^{0.5}$) but the comparison is meaningful since the liquid saturation is not sensitive to the gas flow rate in the explored range as observed in the experiments.

From Fig. 7, we can observe that liquid saturation profiles predicted by numerical simulation do spread in the radial direction. The profile calculated at the highest position $z_1$ shows a maximum displaced from the axis due to the memory of the entrance in the porous zone. In the case we consider a spread factor equal to this obtained from the simplified dispersion model applied to experiments ($S=D_r$), simulations predict globally good order of magnitude for liquid saturations as shown in Fig. 7. However, liquid spreading is still under-estimated comparing to experiences for both cases, b and d. Liquid saturation profiles are actually less spread in the radial direction, particularly at position $z_3$, the farther from liquid entrance. As a matter of fact, $D_r$ gives *a priori* good approximation of spread factor $S$ needed for Euler–Euler model as discussed previously. However, it can be shown theoretically that a ratio $S/D_r=2$ is more relevant with the proviso that a more realistic mass balance than this given in Eq. (13) is considered. This consists in writing the following Eq. (14) instead of Eq. (13) considering non negligible axial velocity derivatives in the radial direction:

$$\frac{\partial q_L}{\partial z}=\underbrace{S\frac{1}{r}\frac{\partial}{\partial r}\left(r|U_{Lz}|\frac{\partial \theta_L}{\partial r}\right)}_{C}=\underbrace{S\frac{1}{r}\frac{\partial}{\partial r}\left(r\frac{\partial q_L}{\partial r}\right)}_{=A}-\underbrace{S\frac{1}{r}\frac{\partial}{\partial r}\left(r\theta_L\frac{\partial |U_{Lz}|}{\partial r}\right)}_{=B}=S(A-B) \qquad (14)$$

Since liquid saturation and liquid velocity magnitude have the same behaviour as regards radial spreading (Figs. 4 and 5), one could expect derivatives denoted C and B in Eq. (14) to have same order of magnitude. This further implies $A\approx 2B$. This has been checked based on simulated liquid saturation profiles and corresponding evaluation of each term (Fourati, 2012). We have numerically the mass balance that leads to $\partial q_L/\partial z\approx S(A/2)=S/2\underbrace{(1/r)(\partial/\partial r)(r(\partial q_L/\partial r))}_{=A}$ while $D_r$ was evaluated experimentally from the equation $\partial q_L/\partial z=D_r\underbrace{(1/r)(\partial/\partial r)\left(r\frac{\partial q_L}{\partial r}\right)}_{=A}=D_rA$.

In order to model liquid spreading using mechanical dispersion force introduced in Section 3.1, one should thus consider a spread factor that is two times greater than this obtained experimentally with a simplified model. This treatment is proved to be consistent since *a posteriori* application of the simplified advection–diffusion model to characterize the dispersion from simulated liquid saturation profiles in case e (Table 1) allowed to calculate a numerical spread factor $D_r$ equal to 3.33 mm that is close to the one determined from experiments (3.7 mm). Based on this argument, a numerical sensitivity analysis as regards $S$ has been carried out. It came out, as expected, that $S=2D_r$ gives most satisfactory results as shown in Fig. 7a for $q_L=16\ \mathrm{m^3/m^2/h}$ and $F_S=1.16\ \mathrm{Pa}^{0.5}$.

Even if we do not report a figure for illustration, we also observed that the liquid distribution predicted by numerical simulations for low and moderate gas flow rates (cases b and d) did not vary significantly in agreement with observations made from experiments.

In order to test if the fractional wetted area participates for a part to the radial distribution of liquid, we included the model giving $f_e$ in case c. Fig. 7b shows that the wetting model does not govern the radial spreading of the liquid as there is no drastic changes between the spatial distribution of liquid predicted in cases b and c. Such behavior was expected since resolution of the non linear algebraic system given by Eqs. (2)–(5) in homogenous conditions and using fractional wetted area-weighted closure laws defined in this work allows calculating fractional wetted areas close to 1 for the range of considered liquid and gas loadings (Fourati, 2012). As far as gas flow rate is concerned, no significant change in liquid saturation profiles is noticed between cases b and d that correspond, respectively to $F_S=1.16\ \mathrm{Pa}^{0.5}$ and $F_S=2.21\ \mathrm{Pa}^{0.5}$. This was expected since tomography measurements revealed no effect of gas flow rate on liquid spreading in Mellapak 250.X packing (Fourati et al., 2012).

Fig. 8a and b provide radial profiles of the velocities in the gas and the liquid phases at different longitudinal positions. In the liquid phase (Fig. 8b), the axial velocity is far larger than this in the radial direction. The liquid jet main direction is the axial one with momentum diffusion in the radial one. This momentum diffusion is linked to dispersion source term in the momentum balance described in Section 3. That does not occur in case a, where no dispersion term is added.

Moreover, gas is also flowing in axial direction mainly (Fig. 8a). In the present simulations, the radial profiles of gas velocity are quite complex. Gas velocity contours in the vicinity of the lower boundary of the column show important accelerations that may be related to the boundary condition at this location and to the inlet of the porous zone (Fig. 9). Boundary conditions associated to counter-current gas–liquid flows are complex to handle but these proposed in this work still give representative results: the saturation and the velocity of the liquid phase as well as the pressure show reasonable distributions even if the gas velocity prediction could be improved.

- Possible model improvements

The discrepancy between the radial profiles of $\theta_L$ predicted by numerics and the more diffusive profiles obtained in the

**Table 2**
Overall pressure drop: simulations vs. experiments.

| Cases | Simulated overall pressure drop (Pa/m) | Experimental overall pressure drop (Pa/m) | Relative error (%) |
|---|---|---|---|
| b | 46.5 | 45 | 3 |
| d | 87.5 | 107 | 18 |
| e | 41.4 | 45 | 8 |

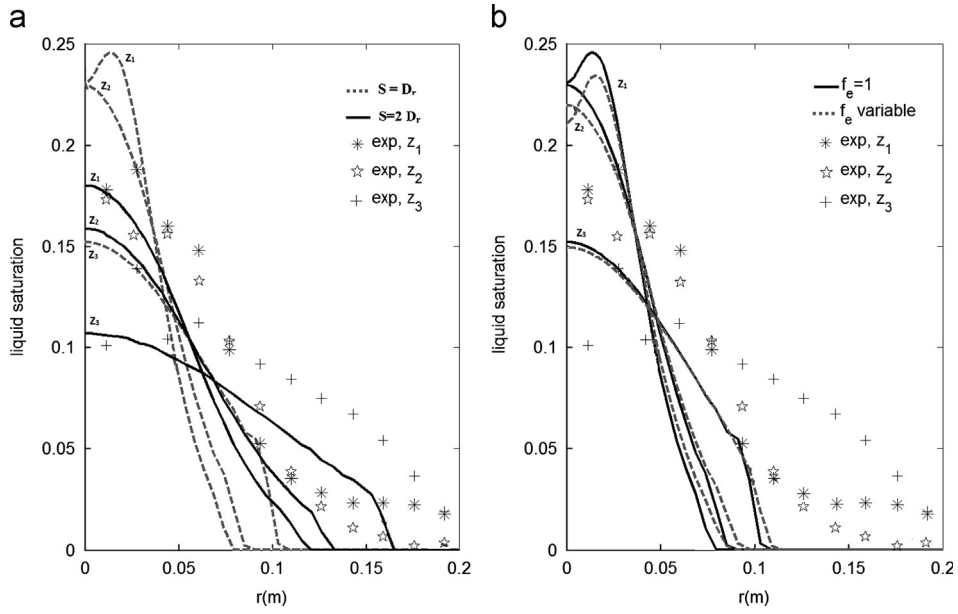


**Fig. 7.** Radial profiles of liquid saturation $\theta_L$ from simulations ($q_L$=16 m$^3$/m$^2$/h, $F_S$=0.74 Pa$^{0.5}$) and experiments ($q_L$=16 m$^3$/m$^2$/h, $F_S$=1.16 Pa$^{0.5}$); a/effect of spread factor (cases b and e of Table 1), b/effect of wetting model (cases b and c of Table 1).

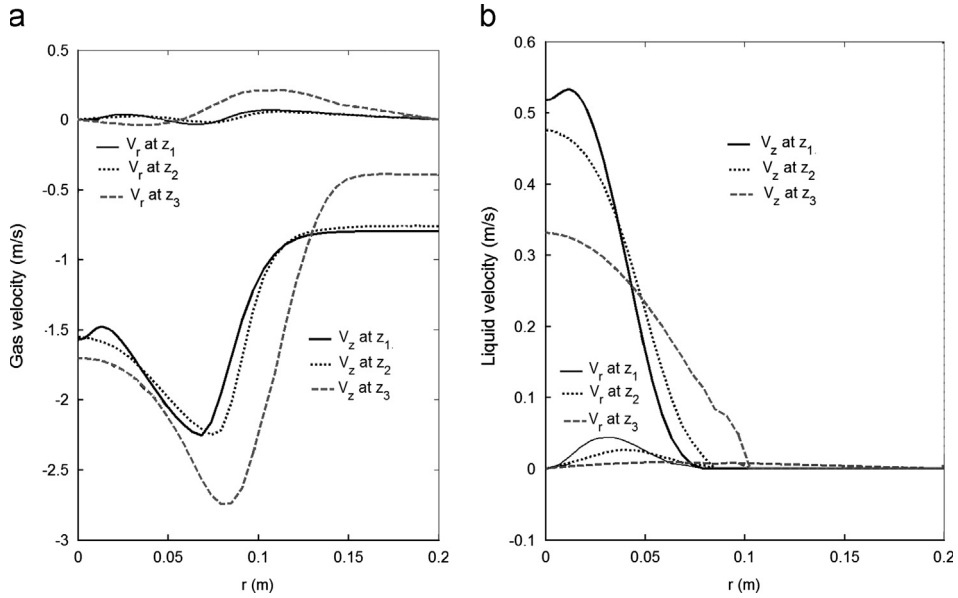


**Fig. 8.** Radial profiles of (a) gas and (b) liquid velocity for simulations: $q_L$=16 m$^3$/m$^2$/h and $F_S$=31.5%$F_C$ (case b in Table 1).

experiments may come from several combined effects, in addition to boundary conditions.

We have checked that the numerical results are not sensitive to the mesh grid in the present numerical conditions. A mesh convergence test has been carried out and has revealed no variation of the flow field when mesh size is increased from 15,200 to 24,800 in terms of cells number.

The knowledge of an exact value of the spreading factor $S$ (and thus $D_r$) may also be crucial for numerical prediction. Concerning this point the experimental method providing the value of $D_r$ should be precisely discussed and tested. In fact, using the experimental correlation $\theta_L = kq_L^{0.4}$ (Eq. (6) in Fourati et al. (2012)) in order to transform measurements of $\theta_L$ into estimations of $q_L$ could introduce artificial distorsion of our estimation of the real spatial distribution of $q_L$. Approximations or uncertainties in the determination of $D_r$ could thus appear. We have checked that numerical results verify, with a satisfactory precision and at any local position, the following relation: $\theta_L = kq_L^{0.4}$. The influence of this transformation is therefore not expected to be a major one.

Moreover, the form of mechanical dispersion force introduced in the work of Lappalainen et al. (2009a) and implemented in simulations does not perfectly match with advection-diffusion model used for calculation of $D_r$ since it assumes zero liquid velocity gradient in the radial direction. A more conservative form of this dispersion force may be a good alternative to model liquid spreading. This gives a dispersion force that is proportional to $\vec{\nabla}(\alpha_L \| \vec{U}_L \|)$ instead of $\| \vec{U}_L \| \vec{\nabla} \alpha_L$. Such alternative has not been explored yet.

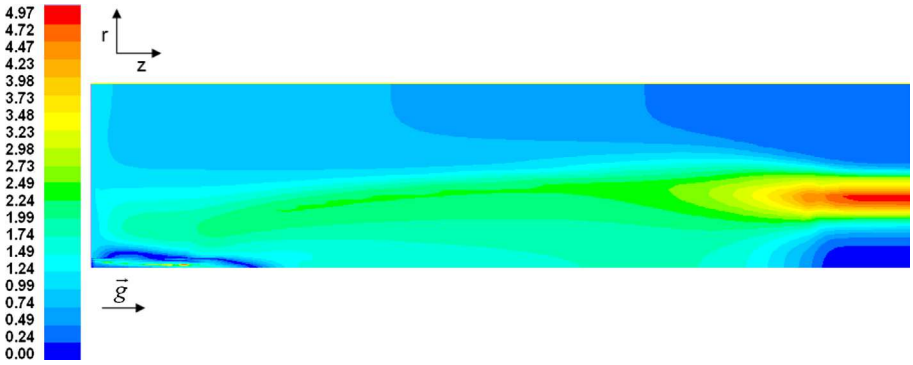


**Fig. 9.** Contours of gas velocity magnitude (m/s): $q_L$=16 $m^3/m^2/h$, $F_S$=31.5%$F_C$ (case b in Table 1).

## 5. Conclusion and perspectives

An Eulerian two-fluid model to predict gas–liquid flows in packed columns has been developed. This model gives a local description of the two-phase flow using volume-averaged quantities. The models of the momentum exchanges at the walls and at the interface between the liquid and the gas are based on the proposal of Iliuta and Larachi (2005). The modeling of liquid dispersion was an important goal of the present study. The model of Lappalainen et al. (2009a) has been adapted and tested for counter-current flow in a structured packing. The comparison of the numerical predictions with recent experimental results obtained in counter-current flow is promising. The difference between experiments and numerics could originate from the selected model of mechanical dispersion. In the absence of firm theoretical basis it is difficult to evaluate the most representative model from Liu and Long (2000) or from Lappalainen et al. (2009a).

## Nomenclature

*Latin letters*

| | |
|---|---|
| $a_g$ | packing external surface area per unit volume of packed bed, $m^2/m^3$ |
| $A_k$ | viscous permeability for phase $k$ |
| $\underline{C_k}$ | coefficient of the inertial isotropic resistance |
| $\overline{\overline{C}}_k$ | inertial resistance tensor for phase $k$ |
| $\underline{D_r}$ | liquid spread factor, m |
| $\overline{\overline{D}}_k$ | viscous resistance tensor for phase $k$ |
| $e$ | liquid film thickness, m |
| $E_1$,$E_2$ | Ergun coefficients |
| $f_e$ | fractional wetted area |
| $F_S$ | gas capacity factor, $Pa^{0.5}$ |
| $F_C$ | gas capacity factor at flooding conditions, $Pa^{0.5}$ |
| $\vec{F}_{\text{disp},k}$ | dispersive term in the momentum equation of phase $k$ |
| $g$ | gravity acceleration, $m/s^2$ |
| $H$ | interface curvature, $m^{-1}$ |
| $h_k$ | width of phase $k$ in a slit, m |
| $K_{IG}$ | coefficient in the law of $\vec{R}_{IG}$ |
| $K_{kS}$ | coefficient in the law of $\vec{S}_{\text{porous},k}$ |
| $\overline{\overline{K}}_L$,$\overline{\overline{K}}_{IG*}$ | dispersion tensors |
| $l_k$ | size of phase $k$ at the pore scale, m |
| $P$ | Pressure, Pa |
| $q_L$ | liquid load, $m^3/m^2/h$ |
| $r$ | radial component in a cylindrical coordinate system |
| $\vec{R}_{Ik}$ | average momentum transfer term at the interface for phase $k$ |
| $\vec{S}_{\text{porous},k}$ | average momentum transfer at the wall for phase $k$ |
| $\underline{S}$ | spread factor (m) |
| $\overline{\overline{S}}$ | spreading tensor |
| $U_{GS}$ | gas superficial velocity, m/s |
| $U_{LS}$ | liquid superficial velocity, m/s |
| $\vec{U}_k$ | intrinsic volume-average velocity of phase $k$, m/s |
| $\vec{U}_{D,k}$ | drift velocity of phase $k$ |
| $z$ | axial component in a cylindrical coordinate system |

*Greek letters*

| | |
|---|---|
| $\alpha_k$ | volume fraction of phase $k$ |
| $\Delta P/\Delta z$ | pressure drop, Pa/m |
| $\varepsilon$ | packing void fraction, porosity, dimensionless |
| $\theta$ | angle with the horizontal direction or azimuthal component in a cylindrical coordinate system |
| $\theta_k$ | saturation of phase $k$ |
| $\mu_k$ | dynamic viscosity of phase $k$, Pa/s |
| $\rho_k$ | density of phase $k$, $kg/m^3$ |
| $\sigma$ | surface tension, N/m |
| $\tau_k$ | tortuosity of phase $k$ |
| $\overline{\overline{\tau_k}}$ | averaged viscous stress tensor in phase $k$ |

*Subscript*

| | |
|---|---|
| C | capillary |
| G | gas phase |
| L | liquid phase |
| s | solid |
| w | wall |

## References


Alix, P., Raynal, L., 2008. Liquid distribution and liquid hold-up in modern high capacity packings. Chem. Eng. Res. Des. 86, 585–591.

Alix, P., Raynal, L., Abbe, F., Meyer, M., Prevost, M., Rouzineau, D., 2011. Mass transfer and hydrodynamic characteristics of new carbon carbon packing: application to $CO_2$ post-combustion capture. Chem. Eng. Res. Des. 89, 1658–1668.

Attou, A., Boyer, C., Ferschneider, G., 1999. Modelling of the hydrodynamics of the cocurrent gas–liquid trickle flow through a trickle-bed reactor. Chem. Eng. Sci. 54, 785–802.

Attou, A., Ferschneider, G., 2000. A two-fluid hydrodynamic model for the transition between trickle a pulse flow in a cocurrent gas–liquid packed-bed reactor. Chem. Eng. Sci. 55, 491–511.

Bacri, J.C., Chaouche, M., Salin, D., 1990. Modèle simple de perméabilités relatives croisées. C. R. Acad. Sci. Paris (Série II) 311 (6), 591–597.

Brenner, H., 1980. Dispersion resulting from flow through spatially periodic porous media. Philos. Trans. R. Soc. 297 (1430), 81–133.

Boyer, C., Koudil, H., Chen, A., Dudukovic, P., 2005. Study of liquid spreading from a point source in a trickle bed via gamma-ray tomography and CFD simulation. Chem. Eng. Sci. 60, 6279–6288.

Brunazzi, E., Paglianti, A., 1997. Mechanistic pressure drop model for columns containing structured packings. AIChE J. 43 (2), 317–327.
Carbonell, R.G., Whitaker, S., 1983. Dispersion in pulsed systems—II Theoretical developments for passive dispersion in porous media. Chem. Eng. Sci. 38 (11), 1795–1802.
Edwards, D.P., Krishnamurthy, K.R., Potthof, R.W., 1999. Development of improved method to quantify maldistribution and its effect on structured packing column performance. IChemE 77 (Part A), 656–662.
Eidsath, A., Carbbonell, R.G., Whitaker, S., Herrmann, L.R., 1983. Dispersion in pulsed systems—II Comparison between theory and experiments for packed beds. Chem. Eng. Sci. 38 (11), 1803–1816.
Ergun, S., 1952. Fluid flow through packed columns. Chem. Eng. Prog. 48 (2), 89–94.
Fourati, M., Roig, V., Raynal, L., 2012. Experimental study of liquid spreading in structured packings. Chem. Eng. Sci. 80, 1–15.
Fourati, M., 2012. Dispersion de liquide dans des écoulements gaz-liquide à contre-courant dans des colonnes à garnissages: étude expérimentale et modélisation numérique. Ph.D. Thesis. University of Toulouse.
Grosser, K., Carbonell, R.G., Sundaresan, S., 1988. Onset of pulsing in two-phase cocurrent downflow through a packed bed. AIChE J. 34 (11), 1850–1860.
Holub, R.A., Dudukovic, M.P., Ramachandran, P.A., 1993. Pressure drop, liquid holdup and flow regime transition in trickle flow. AIChE J. 39 (2), 302–321.
IEA, 2009. Ed. Available at 〈http://www.iea.org/papers/2009/CCS_Roadmap.pdf〉.
Iliuta, I., Larachi, F., Al-Dahhan, M.H., 2000. Double-slit model for partially wetted trickle flow hydrodynamics. AIChE J. 46 (3), 597–609.
Iliuta, I., Petre, C.F., Larachi, F., 2004. Hydrodynamic continuum model for two-phase flow structured-packing-containing columns. Chem. Eng. Sci. 59, 879–888.
Iliuta, I., Larachi, F., 2005. Modelling the hydrodynamics of gas–liquid packed beds via slit models: a review. Int. J. Chem. Reactor Eng. 3, 4, Review.
Jiang, Y., Khadilkar, M.R., Al-Dahhan, M.H., Dudukovic, M.P., 2002. CFD of multi-phase flow in packed-bed reactors: I. k-Fluid modeling issues. AIChE J. 48 (4), 701–715.
Lappalainen, K., Manninen, M., Alopaeus, V., 2009a. CFD modelling of radial spreading of flow in trickle-bed reactors due to mechanical and capillary dispersion. Chem. Eng. Sci. 64, 207–218.
Lappalainen, K., Manninen, M., Alopaeus, V., Aittamaa, J., Dodds, J., 2009b. An analytical model for capillary pressure–saturation relation for gas–liquid system in a packed-bed of spherical particles. Transp. Porous Media 77, 17–40.
Lappalainen, K., Gorshkova, E., Manninen, M., Alopaeus, V., 2011. Characteristics of liquid and tracer dispersion in trickle-bed reactors: effect on CFD modelling and experimental analyses. Comput. Chem. Eng. 35, 41–49.
Liu, S., 1999. A continuum approach to multiphase flows in porous media. J. Porous Media 2 (3), 295–308.
Liu, S., Long, J., 2000. Gas–liquid countercurrent flows through packed towers. J. Porous Media 3 (2), 99–113.
Macdonald, I.F., El-Sayed, M.S., Mow, K., Dullien, F.A.L., 1979. Flow through porous media: the Ergun equation revisited. Ind. Eng. Chem. Fundam. 18 (3), 199–208.
Menon, A., Duss, M., 2011. Reducing the energy penalty for post-combustion $CO_2$ capture. Carbon Capture J. 23, 2–5.
Mewes, D., Loser, T., Millies, M., 1999. Modelling of two-phase flow in packings and monoliths. Chem. Eng. Sci. 54, 4729–4747.
Olujic, Z., Kamerbeek, A.B., De Graauw, J., 1999. A corrugation geometry based model for efficiency of structured distillation packing. Chem. Eng. Process. 38, 683–695.
Prieur Du Plessis, J., 1994. Analytical quantification of coefficients in the Ergun equation for fluid friction in a packed bed. Transport in Porous Media 16, 189–207.
Quintard, M., Whitaker, S., 1993. Transport in ordered and disordered porous media: volume-averaged equations, closure problems and comparison with experiments. Chem. Eng. Sci. 48 (14), 2537–2564.
Raynal, L., Royon-Lebeaud, A., 2007. A multi-scale approach for CFD calculations of gas–liquid flow within large size column equipped with structured packing. Chem. Eng. Sci. 62, 7196–7204.
Raynal, L., Bouillon, P.A., Gomez, A., Broutin, P., 2011. From MEA to demixing solvents and future steps, a roadmap for lowering the cost of post-combustion carbon capture. Chem. Eng. J. 171, 742–752.
Tsai, R.E., Seibert, A.F., Eldridge, R.B., Rochelle, G.T., 2011. A dimensionless model for predicting the mass-transfer area of structured packing. AIChE J. 57 (5), 1173–1184.
Vafai, K., 2005. Dispersion in Porous Media. In: Liu, S., Masliyah, J.H. (Eds.), Handbook of Porous Media. CRC Press, Taylor and Francis Group.
Valdes-Parada, F.J., Ochoa-Tapia, J.A., Alvarez-Ramirez, J., 2009. Validity of the permeability Carman–Kozeny equation: a volume averaging approach. Physica A 388, 789–798.
Weimer, T., Schaber, K., 1996. Determination of effective interfacial areas by absorption of carbon dioxide from air. Chemische Technik 48 (5), 241–249.
Whitaker, S., 1996. The Forcheimer equation: a theoretical development. Transport in porous media 25, 27–61.
Whitaker, S., 1973. The transport equations for multi-phase systems. Chem. Eng. Sci. 28, 139–147.
Whitaker, S., 1986. Flows in porous media II: The governing equations for immiscible, two-phase flow. Transp. Porous Media 1, 105–125.
Whitaker, S., 1999. The Method of Volume Averaging. Kluwer Academic Publishers, Dordrecht.